Modelling and Analysis of a Combined Electronic and Micro-mechanical System

Maja Atanasijević-Kunc[1,*] - Vinko Kunc[2] - Janez Diaci[3] - Rihard Karba[1]
[1] University of Ljubljana, Faculty of Electrical Engineering, Ljubljana, Slovenia
[2] IDS d.o.o. Integrated circuits, Ljubljana, Slovenia
[3] University of Ljubljana, Faculty of Mechanical Engineering, Ljubljana, Slovenia

The modelling of micro-mechanical systems in combination with integrated electronic circuits is a complex task demanding a knowledge of mechanical and microelectronic design in combination with system-modelling expertise, especially in cases where new possibilities regarding system construction and its properties are taken into account. Such modelling is becoming increasingly important because of the rapid growth of so-called "smart sensor" applications based on micro-mechanical devices. Our task was to create a reliable model of a micro-mechanical acceleration sensor that uses an extremely small and easy-to-produce mechanical system. The suspended mass and the output signal of this sensor are one order of magnitude smaller than existing systems. The described model was used for the further development of the mechanical and electrical parts of the system. The modelling inputs were the measurement data of the prototype devices, comprising the static characteristics of the device and the system responses to step-function excitation. Together with known physical properties and basic theoretical equations these data enabled us to create the described model, which showed good agreement with the measurement results.
Keywords: micro-mechanical system, modelling, acceleration sensor, control design

0 INTRODUCTION

Micro-mechanical devices are mechanical systems where the sizes of the features are in the micron or even sub-micron range. These devices are produced using techniques that are similar to those used in micro-electronic production; this makes the two technologies very compatible. The micro-mechanical system can be a stand-alone element or it can be realized as an integral part of the micro-electronic system. The result is a system comprising an electrical part that is capable of the complexity offered by the existing capabilities of micro-electronic technology and a mechanical part that can be produced with extremely precise dimensions.

If the mechanical part is a stand-alone element it is normally produced using a bulk micro-machining technology. This technology enables three-dimensional mechanical design, where the dimensions of the suspended element are in μm and the mass is measured in mg [9], [12], [15] and [16]. More recent systems use a surface micro-machining technology, where the mechanical part is produced on top of the electronics in the post-processing steps

following the usual production of micro-electronic devices [2], [3] and [5]. There are, however, severe limitations imposed on the surface of the micromachined mechanical part due to currently available production techniques. The choice of material for the mechanical part is mainly limited to silicon and silicon oxide, and the geometry of the mechanical design is predominantly two dimensional as the thickness of the element is limited to a few μm. Of course the suspended mass in such systems is much smaller than that of bulk micro-machined devices and is typically in the range of μg.

The system described in the paper goes one step further. To ensure minimum production costs, which is a very important aspect of the design, the mechanical part is reduced to a single cantilever with extremely small dimensions (490 x 211 x 0.9 μm). The resulting suspended mass is only 0.23 μg, which is 3-4 orders of magnitude lower than bulk micro-machined devices and an order of magnitude lower than typical surface micro-machined devices.

Also the capacitive position sensing is much more demanding in the described system

*Corr. Author's Address: University of Ljubljana, Faculty of Electrical Engineering, Tržaška 25, SI-1000 Ljubljana, Slovenia, maja.atanasijevic@fe.uni-lj.si

due to the extremely small dimensions. The capacitance of the sensing capacitor in the case of bulk micro-machined devices is typically 10-20pF, and in the case of surface micro-machined devices it is typically 1-2pF. In the described system the sensing capacitor's capacitance is only 0.1pF.

In our case the situation was made worse because the described system only uses a one-sided sensing capacitor, while typical solutions make use of differential capacitive sensing [2], [3], [5], [9], [12], [14] and [16]. To cope with the problem of an extremely small mechanical device we had to construct a system model that would be reliable and accurate enough for engineering purposes, while still suitable for a complete system simulation that involves both open and closed-loop operation with pulse-width-modulated electrostatic force feedback.

1 MATHEMATICAL SYSTEM MODELLING

The development of the model can be divided into two main phases. In the first phase a theoretical model based on the proposed geometry of the mechanical part and the physical properties of the material used was constructed. To make this model usable in practise for the simulation and animation it had to be simplified and transformed into a discrete-element system with the minimum degradation of model performance. This model provided the basic data on the predicted performance of the mechanical part, which was then translated to the required specifications for the electronic part of the system. The electronic design team was able to meet the demands made by the extremely small signal of the sensor (approximately 50 electrons resolution in a 200Hz signal bandwidth) so the production of prototype samples was started.

The second modelling phase applied the measurements of the prototype samples for model improvement. The improved model showed good matching with the measurement results, which gave us the confidence to belive it could be used for further development of the measurement system. This model was later successfully used for closed-loop system development comprising pulse-width electrostatic feedback and variations of the system with different measurement ranges.

1.1. The Theoretical Model

The geometry of the mechanical part was governed mainly by the desire for simple and cheap production of the sensor system. This limited the mechanical system to a single cantilever of 490 μm in length, 211 μm wide and 0.9 μm thick. At one end it was attached to the bulk silicon, and at the other end it was free to move. The cantilever beam was placed above the measurement electronics, comprising three capacitor plates forming capacitance to the beam. The beam was electrically connected to the ground node of the measurement electronics. The basic physical situation is presented in Fig. 1, which shows a cross-section of the micro-mechanical measurement system.
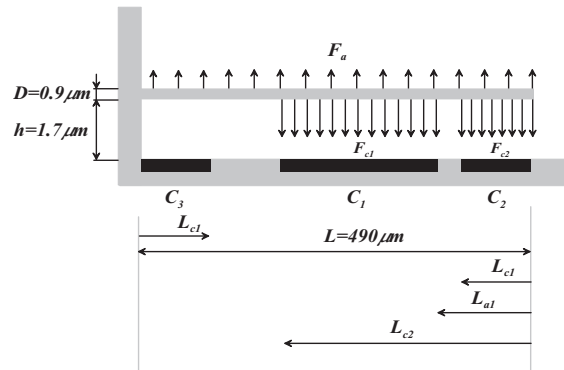

Fig. 1. *The cross-section of the micro-mechanical system*

Two capacitor plates form variable capacitors, with the beam acting as a grounded electrode. One capacitor (C_2 in Fig. 1) was used as a distance-measurement capacitor. In combination with capacitor 1 (C_1 in Fig.1) it was also used to apply an actuation force. Capacitor 3 (C_3 in Fig.1) was used only to verify the distance of the beam from the silicon surface.

The dynamics of the cantilever motion can generally be described by the following partial differential equation [13] (see Fig. 2):

$$\rho DB \ddot{y}(x,t) + q_{\mathrm{d}}(\dot{y},y,x,t) + EI\frac{\partial^4 y(x,t)}{\partial x^4} =$$
$$q_{\mathrm{c1}}(y,x,t) + q_{\mathrm{c2}}(y,x,t) - \rho DB\alpha(t) \qquad (1)$$

Anatisijević-Kunc, M. - Kunc, V.- Diaci, J.- Karba, R.

with the boundary conditions:

$$y(L,t) = 0; \qquad \frac{\partial y(L,t)}{\partial x} = 0$$

$$\frac{\partial^2 y(o,t)}{\partial x^2} = 0; \qquad \frac{\partial^3 y(0,t)}{\partial x^3} = 0$$

where:

$y(x, t)$ is the deflection of the beam at distance x from the tip;

ρ, D, B, L are the beam density, thickness, width and length;

E is the Young's modulus for silicon;

I is the area moment of inertia;

q_d, q_{c1}, q_{c2} are distributed loads (force per unit length);
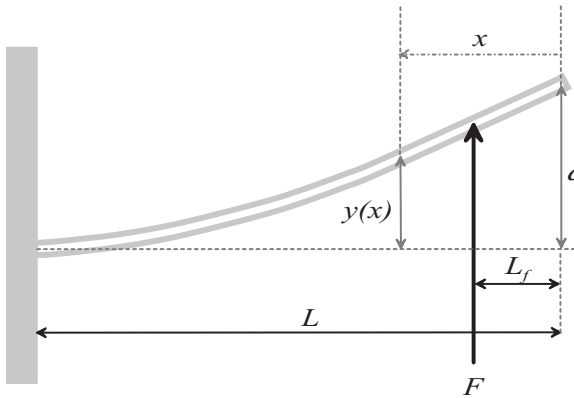
$a(t)$ is the acceleration of the system.

Fig. 2. *Cantilever deflection*

The distributed electrostatic forces q_{c1} and q_{c2} are of the form:

$$q_{ci}(y,x,t) = \frac{1}{2}\varepsilon B U_{ci}^{2} \frac{\Pi(x,L_{ci},L_{a1})}{\left(h + y(x,t)\right)^2}$$

with

$$\Pi(x,L_{ci},L_{a1}) = \begin{cases} 1 & for \quad 0 \le x \le L_{c1} \\ 1 & for \quad L_{a1} \le x \le L_{c2} \\ 0 & elsewhere \end{cases}$$

where index $i=1$ designates the first, $i=2$ the second capacitor, and h is the distance of the unloaded beam above the bottom surface.

The distributed damping load, q_d, can be determined from another partial differential equation [4,8,18] describing the motion of the gas (air) below the beam, which is induced by the motion of the beam.

In order to obtain the beam deflection $y(x,t)$, which is the basis for determining the output voltage, it would be necessary to numerically solve a highly non-linear system of partial differential equations, which is not suitable for dynamic simulation purposes [10].

To overcome this problem we have discretized the beam into twenty equidistant segments ($L_s=L/20$), and approximated the equation (1) with the corresponding boundary conditions, using the following assumptions:

$$y(x,t) \approx y\left(x_j,t\right) = y_j(t)$$

$$\frac{\partial y\left(x_j,t\right)}{\partial x} \approx \frac{1}{2L_s}\left[y_{j+1}(t) - y_{j-1}(t)\right]$$

$$\frac{\partial^2 y\left(x_j,t\right)}{\partial x^2} \approx \frac{1}{L_s^{2}}\left[y_{j+1}(t) - y_j(t) + y_{j-1}(t)\right]$$

$$\frac{\partial^3 y\left(x_j,t\right)}{\partial x^3} \approx \frac{1}{2L_s^{3}}\left[y_{j+2}(t) - 2y_{j+1}(t) + \right.$$
$$\left. + 2y_{j-1}(t) - y_{j-2}(t)\right]$$

$$\frac{\partial^4 y\left(x_j,t\right)}{\partial x^4} \approx \frac{1}{L_s^{4}}\left[y_{j+2}(t) - 4y_{j+1}(t) + \right.$$
$$\left. + 6y_j(t) - 4y_{j-1}(t) + y_{j-2}(t)\right].$$

The result was a set of ordinary differential equations of the form:

$$m_s \ddot{y}_j(t) + b_j\left(y_j\right)\dot{y}_j(t) + k_s\left[y_{j+2}(t)\right.$$
$$-4y_{j+1}(t) + 6y_j(t) - 4y_{j-1}(t) + y_{j-2}(t)\left.\right] =$$
$$= F_{cj} - F_{aj}(t)$$
$$j = 1,2,3,\cdots,20 \tag{2}$$

where the meaning of the notation in (2) is the following:

$F_{cj}(t)$ is the electrostatic (point) force acting upon the j-th beam segment,

$F_{aj}(t) = m_s a$ is the acceleration force,

$m_s = \rho D B L_s$ is a segment mass,

$k_j = E I / L_s^{3}$ is the characteristic spring stiffness,

$b_j(y_j)$ is a damping coefficient; the damping element was omitted only at the tip segment to meet the boundary conditions.

The air-gap width between the cantilever and the silicon surface is extremely small (1.7 μm) compared to the cantilever width (211 μm). This implies that the air cannot move freely. In order to determine the damping coefficients b_j we employed the squeeze-film-damping model [18]. The basic equation of damping by an air-film squeezed between two rectangular plates is:

$$b_j\left(y_j\right)=\frac{\mu B^3 L \alpha\left(B/L\right)}{h^3\left(1+\dfrac{y_i}{h}\right)^3}$$

(3)

where μ is the dynamic (absolute) viscosity, and α is a geometry-dependent constant [18]. This formula is strictly valid only for the parallel motion of the two plates. We estimated however that this relation contains the relevant parameters and is dimensionally correct also for the spatially variable gap geometry. We also expected that we could, if necessary, modify the equation on the basis of experimental data.

The nonlinear model of the mechanical part is therefore of the 40th-order and represents in our view a suitable compromise between the requirement for accurate modelling of the relevant physical phenomena (distributed nonlinear loads, distributed detection) and the computational resources at our disposal.

1.2 The Electronic Part of the System

The design of the electronic part was mainly driven by the demand for a precise and low-noise position-measurement system. To enable simple production of the mechanical system the beam is electrically connected to the sensor-chip substrate and thus to the ground potential. The noise analysis of the system indicated that the most effective input structure would, in our case, be a simple capacitive divider, because we are using only one electrode to measure the capacitance. The capacitive divider consists of the capacitance between the sensing electrode and the grounded beam (C_x) and the excitation signal supplying the capacitor (C_r) connected between the sensing electrode and a source of the AC signal (excitation signal), as shown in Fig. 3 where the meaning of the marks is the following:

1 – grounded cantilever
2 – voltage follower system

3 – phase selective sampling
4 – subtraction and DC adjust
5 – gain
6 – DC adjust control
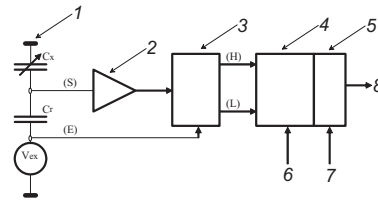7 – gain control
8 – position output

Fig. 3. *Electronical part of the system*

The beam-tip position displacement changes the capacitance of the sensing electrode to the beam (C_x - capacitor 2) and thus influences the amplitude of the signal on the node S. It can be described with the following:

$$U_S=\frac{U_E C_r}{\left(C_r + C_x\right)}$$

(4)

where U_E is the peak-to-peak value of the excitation signal. Node S is a node with an extremely high impedance, so the voltage of this node cannot be directly accessed. To observe the voltage of this node a special patented voltage-follower system was designed, having only a 1fF (10^{-15}F) effective input capacitance. This was a key parameter, as the capacitance of both capacitors in the divider system does not exceed 90fF and a higher follower input capacitance would drastically reduce the available signal.

The output of the voltage follower is further processed in a system where the upper and lower peak values of the signal are sampled (signals (H) and (L)). The voltage difference of both signal peaks is calculated in next signal-processing step and the DC offset is removed using zero-position adjustment. The electronic position-measurement system thus basically transforms the displacement of the beam tip to a change in the peak-to-peak voltage of the divided excitation signal, which is further converted to a direct voltage output by means of peak-to-peak sampling. The high-level model of the electronic system must reflect three main parameters of the real electronic system.

- The first is the nonlinearity of the transformation from beam-position change

to output voltage. The change in the beam position is reflected in the change of the peak-to-peak voltage swing on node (*S*), as described in (4). This parameter is inherent in the system we are using and we can only influence it by changing the mechanical properties of the system, i.e., the distance of the beam from the measurement electrode and the stiffness of the beam. Of course the improvements in open-loop linearity (bigger distance and stiffer beam) cause a reduction of the sensitivity, and so the optimum had to be found. The linearity is not a problem in a closed-loop system as it can be greatly improved by the feedback control.

- The second is the delay of the electronic processing of the signal. This is mainly dependent on the frequency of the AC excitation signal, as the peak-to-peak measurement system requires at least one clock cycle of the AC signal to display the correct output value. Of course we want the delay to be as short as possible, especially in the case of closed-loop realization, due to potential stability problems. For this we have to increase the frequency of the AC excitation signal, where the limitation is the settling time of the voltage-follower amplifier.

- The third is the gain (*K*). For an open-loop measurement system it must be chosen so that the output-voltage swing covers the desired measurement range. In the closed-loop configuration it influences the level of system linearity and signal bandwidth. The obvious limitations are the system stability and the increase of the noise level in the loop.

For a complete system description and simulation the model of the electrical part has to be merged with the model of the mechanical part, as the properties of the electrical part can significantly influence the overall system behavior. For this reason we have decided to include in the model description all three mentioned parameters. The non-linearity of the system is incorporated through (4). The measurement-system delay, which is equal to one period of the excitation signal, was taken to be 50 µs, as this is an optimal value coming from transistor-level simulations of the

measurement electronics [6] and [7]. The gain (*K*) is a parameter that we can choose to suit the system requirements. So the function of the beam deflection to the output voltage of the measurement system can be defined as:

$$U_{\text{out}} = K \frac{U_{\text{E}} C_{\text{r}}}{\left(C_{\text{r}} + \dfrac{\varepsilon A_2}{h + y(z)} \right)} \qquad (5)$$

and the output is sampled every 50 µs. In (5) ε is the dielectric constant and A_2 is the area of the capacitor 2 (see Fig.2).

We should mention that the functionality and the desired properties of the electrical part itself were optimized with a simulation in SPICE [6] and [7].

1.3 Comparison of the Model to the Measurement Results

The experiments with the prototype samples were divided into observations of the static and dynamic properties. First, the electrostatic actuator system was used to apply a force to the cantilever. This system uses both capacitors in the middle and at the tip to apply the attraction force to the beam. Since the capacitor beneath the beam tip is also used for the distance measurement, the actuation and measurement function are multiplexed on the same capacitor. This results in a 50% duty ratio of actuation, which was also included into the model for force calculations. The measurements of the beam-tip deflection as a result of the electrostatic force are presented in Table 1.

Table 1. *Static characteristics of the combined system*

Actuation voltage [V]	Output voltage [V]	Tip capacitance value	Calculated applied force on the tip	Cantilever tip distance to surface	Relative position [nm]
0.0	0.00	84.86	0+11	2204	0
0.3	-0.10	85.04	1+11	2199	5
0.6	-0.28	85.37	4+11	2190	14
0.9	-0.99	86.71	9+11	2157	47
1.2	-1.74	88.15	17+12	2121	83
1.5	-2.67	90.01	28+12	2078	126
1.8	-3.91	92.58	42+13	2019	185
2.1	-5.58	96.25	62+14	1943	261
2.4	-8.13	102.2	90+16	1829	375

The actuation voltage in the first column is the voltage applied to the actuation capacitors. The output voltage is the output of the tip-capacitor measuring system. The third column represents the calculated capacitance value of capacitor number 2. The fourth column shows the calculated applied force on the cantilever tip from the actuation capacitors and from the measurement system (the excitation voltage used for the capacitance measurement also exhibits electrostatic force). Knowing the characteristics of the capacitance-measurement electronics the cantilever-tip distance to the silicon surface was then calculated as presented in the fifth column.

The described data were used to improve the static properties of the mechanical part of the model. Comparing these results to the model the obvious difference was the starting position of the cantilever. In the real system the beam was bent back so that the beam tip was 0.5 μm further from the surface than the core of the beam. This is the result of residual stress caused by the production procedure of the cantilever. To implement this in the model we applied a pull-up force along the whole cantilever length, which resulted in the beam bending observed in the measurements. We also made minor changes to the beam stiffness to fit the model to the measurements. These differences could result from the fact that the beam material was polycrystalline silicon, and from the uncertainty of the beam thickness.

The dynamic response of the system was also measured using the actuation voltage as the input stimulus. The actuation voltage was changed step-wise by 350 mV at different DC starting points of the actuation voltage. The DC starting actuation voltage created an attraction force so the beam position at the start of each step function (350 mV amplitude) was different for each measurement. The capacitance change at the beam tip, as measured by the position-sensing electronic system, was observed using a digital oscilloscope. The step change in the actuation voltage resulted in an increase of the attraction force as the capacitor voltage was increased. This additional force required a change in the beam-tip position to compensate the new value of the electrostatic force with the spring force of the cantilever. The beam movement was, of course, damped by the air-damping mechanisms. The oscilloscope shots (as shown in Figs. 4 and 6) present the time-dependent movement of the beam tip.

These results were compared to the theoretical model. Here, the differences between the model and the measurement results were bigger compared to the static measurements of the system. The measurement results showed that the damping factor was increased by more than a factor of two if the cantilever position was moved from 2204 to 1829 nm. This is an even higher ratio than the theoretically calculated factor of 1.73. This led us to the conclusion to use (in Eq. (3) in denominator) the dimensionless-gap width to the power of four in our damping calculations.

The improved model showed very good agreement with the measurement results over the whole operating range of the system, which is illustrated with two pairs of figures. In the first pair (Figs. 4 and 5) the system responses are presented for an input voltage change from 359 to 13mV. In Fig. 4 the oscilloscope plots are illustrated.
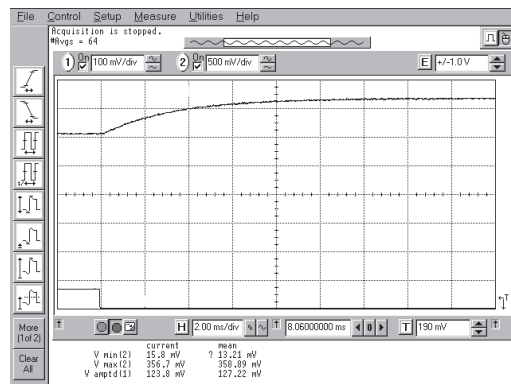

Fig. 4. *Oscilloscope plots of the transient response caused by the actuation-voltage change from 359 to 13 mV*
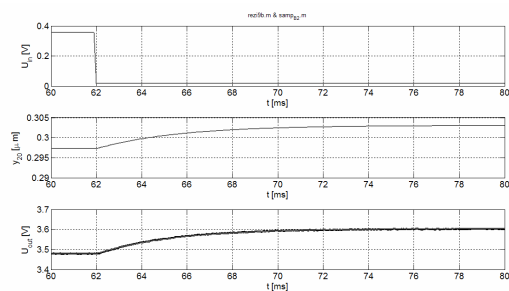

Fig. 5. *Transient responses of the model in comparison with the measurement data for the actuation-voltage change from 359 to 13 mV*
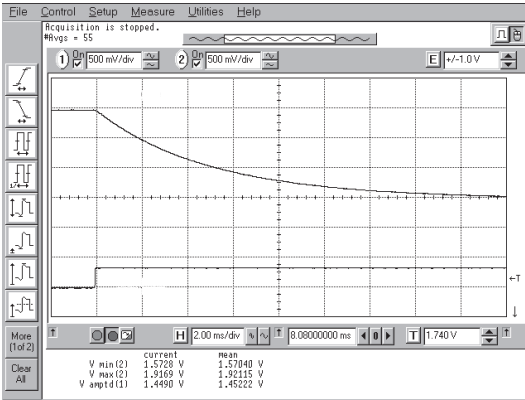
Fig. 6. *Oscilloscope plots of the transient response caused by the actuation-voltage change from 1.57 to 1.921V*
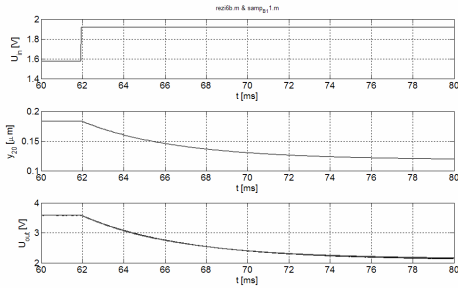

Fig. 7. *Transient responses of the model, in comparison with the measurement data, caused by the actuation-voltage change from 1.57 to 1.921V*

The oscilloscope plots present the response of the cantilever-tip position-measurement electronics as the upper trace (trace 1), and the actuation voltage as the lower trace (trace 2). The measurements below show the lower voltage level of the actuation voltage (Vmin(2)), the higher level of the actuation voltage (Vmax(2)) and the resulting difference of the position-measurement signal (Vamptd(1)). The input stimuli is a step-voltage change in the actuation voltage and the levels are Vmin(2) and Vmax(2). The time scale in all the plots is 2 ms per division.

Fig. 5 is divided into three subplots, where it is possible to observe the applied input voltage (upper part), the movement of the cantilever tip (middle part) and the corresponding output-voltage signal (lower part) of the model. In this lower part of the plot the measurement data from

Fig. 4 are also presented in black color, while model responce is gray. A similar comparison of the model and the system responses are presented in Fig. 6 and 7 for an input voltage-change from 1.57 V to 1.921 V.

We should mention that the simulation of the described measurement system and the animation of the mechanical part were realized in Matlab with Simulink [11] and [17].

2 SUMMARY

The model of the presented micro-mechanical system was a team effort by specialists in the field of microelectronic design, mechanical design and control. It was developed in a cyclic procedure, where the introduced simplifications made it possible to include the whole system in the same simulation environment. Several iterations were needed because all of the system properties and parameters were not known in advance.

The starting model was based on theoretical equations and was further improved using measurement data taken from prototype devices. The development of the model involved two major steps.

The first step covered the static characteristics of the system resulting from the equilibrium of the electrical actuation force and the cantilever spring force.

The second step was the introduction of the dynamic properties governed mainly by air-damping mechanisms. The final result has a high degree of compliance with the actual measurements and has been used for the further development of the measurement system.

This model was used in the development of a closed-loop measurement system, where the beam-tip position is kept at a constant distance by the electrostatic actuator using pulse-width modulation to adjust the force. The acceleration force is measured by the amount of electrostatic force needed to keep the equilibrium position of the beam tip. The model is also being used to develop an acceleration sensor for low acceleration values where the cantilever stiffness and gas pressure are optimized for the best performance.

3 REFERENCES

[1] Atanasijević-Kunc, M., Kunc, V., Diaci, J., Karba, R., Modelling and Analysis of Combined Electronic and Micro - Mechanical System, *Proceedings of the 4th IMACS Symposium on Mathematical Modelling*, Troch, I., Breitenecker, F. (ed.), Vienna, Austria, 2003.

[2] Baschirto, A. Gola, A., Chiesa, E., Lasalandra, E., Pasolini, F., Tronconi, M., Ungaretti, T., A ±-g dual-axis linear accelerometer in a standard 0.5-μm CMOS technology for high-sensitivity applications, *IEEE Journal of Solid-State Circuits*, July 2003, vol.38, p.1292-1297.

[3] Boser, B. E., Howe, R. T., Surface micromachined accelerometers, *IEEE Journal of Solid-State Circuits*, March 1996, vol.31, p.366-375.

[4] Daugherty, R. L., Franzini, J. B., Finnemore, E. J., Fluid Mechanics with Engineering Applications, *McGraw - Hill*, 8th ed., Singapore, 1985.

[5] Gola, A., Chiesa, E., Lasalandra, E., Pasolini, F., Tronconi, M., Ungaretti, T., Baschirotto, A., Interface for MEMS-based rotational accelerometer for HDD Applications with 2.5 rad/s² resolution and digital output, *IEEE Sensors Journal*, August 2003, vol.3, no.4.

[6] HSPICE, Version H92, Elements and Models, User's Manual, *Meta-Software*, 1992.

[7] HSPICE, Version H92, Analysis and Methods, User's Manual, *Meta-Software*, 1992.

[8] IJntema, D. J., Tilmans, H. A. C., Static and dynamic aspects of an air-gap capacitor, *Sensors and Actuators*, 1992, A, 35, p.121-128.

[9] Marco, S., Samitier, J., Herms, A., Morante, J. R., Analysis of electrostatic - damped piezoresistive silicon accelerometers, *Sensors and Actuators*, 1993, A37 - 38, p.317-322.

[10] Matko, D., Karba, R., Zupančič, B., Simulation and modeling of continuous systems, A case study approach, *Prentice Hall*, 1992.

[11] MATLAB, The Language of Technical Computing, Version 5, *The MathWorks Inc*., 1999.

[12] Matsumoto, Y., Esashi, M., Integrated capacitive accelerometer with novel electrostatic force balancing, *Technical Digest of the 11th Sensor Simposion*, 1992, p.47-50.

[13] Popov, E. P., Engineering Mechanics of Solids, *Prentice Hall*, , 1990, New Jersey.

[14] Rudolf, F., Jornod, A., Bencze, P., Silicon microaccelerometer, Transducers'87, 1987, p.395-398.

[15] Rudolf, F., Jornod, A., Bergqvist, J., Leuthold, H., Precision accelerometers with μg resolution, *Sensors and Actuators*, , 1990, A21-A23, p.297-302.

[16] Siedel, H., Riedel, H., Kolbeck, R., Mück, G., Kupke, W., Königer, M., Capacitive silicon accelerometer with highly symetrical design, *Sensors and Actuators*, , 1990, A21-A23, p.312-315.

[17] Simulink, User's Guide, *The MathWorks Inc*. 1999.

[18] Starr, J. B., Squeeze-film Damping in Solid-State Accelerometers, *IEEE Solid-State Sensor and Actuator Workshop*, , June 1990, Hilton Head Island, p.44-47.